Measurement of Long-Period, Low-Amplitude Swell in the Western North Atlantic Ocean

GLENN D. HAMILTON

National Data Buoy Center, Stennis Space Center, Mississippi

(Manuscript received 10 October 1991, in final form 13 March 1992)

ABSTRACT

Nineteen data buoys in the western North Atlantic and two coastal stations reported 20-s-period swell in August 1990. The source of this very unusual event was traced to a severe storm off the Antarctic continent. This paper provides information on the wave-measuring systems, observations, meteorological conditions that generated the swell, and techniques used to estimate the location of the source of the swell. The swell was measured by different hull types, wave-measuring systems, and electronic payloads. The observations show how wave conditions vary with location and provide data for wave-modeling purposes and research studies.

1. Introduction

In the western North Atlantic Ocean, the National Data Buoy Center (NDBC) operates a chain of moored buoys as part of its national buoy network (for further information see Hamilton 1986). All 13 operational buoys in this region reported distinct 20-s-period wave energy in August 1990. Two NDBC east coast Coastal-Marine Automated Network (C-MAN) fixed stations and six Canadian buoys, south of Newfoundland and Nova Scotia, also measured this swell energy. Figure 1 shows the locations of the buoys and C-MAN stations. The entire region during this time was remarkably calm with significant wave heights of about 1.0 m. This event of long-period, low-amplitude swell might have gone unnoticed, except that records were set for many stations when they reported 20-s dominant periods for the first time, even though they had been established for many years.

According to Pierson et al. (1955), 50-kt (26 m s^{-1}) winds are required to generate 20-s-period waves in a fully developed sea. In Mitsuyasu (1981), the dimensionless variables of spectral peak frequency $\tilde{f}$ and fetch $\tilde{F}$ are represented by

$$\tilde{F} = gF/U^2, \tag{1}$$

$$\tilde{f}_m = Uf_m/g, \tag{2}$$

where g is the acceleration of gravity, U is the wind speed at a 10-m height, f_m is the spectral peak frequency, and F is the effective fetch. A relation was then obtained:

$$\tilde{f}_m = 3.16\tilde{F}^{-1/3}. \tag{3}$$

In section 4, it is estimated that the fetch F of the swell-generating storm was about 1000 km and wind speed U near 26 m s^{-1}. Using these in Eq. (1) and applying the derived value for $\tilde{F}$ in Eq. (3), f_m can be deduced. Inserting this value of $\tilde{f}_m$ into Eq. (2), a value of f_m is calculated to be 0.0486 Hz, giving a peak period of 20.5 s.

Examination of weather maps for the North Atlantic for the previous week revealed that there were no storms that could have generated such long-period waves. The question arose as to whether the swell could have been generated in the Southern Hemisphere. Munk et al. (1963) and Snodgrass et al. (1966) reported on swell arriving at the California coast from the South Pacific Ocean. Barber and Ursell (1948) described long-period swell with a characteristic period of about 21 s that had been generated near Cape Horn and arrived off the English coast. Ewing (1971) discussed the propagation of these swell waves in terms of the laws of linear hydrodynamics. The author knows of no articles that report Southern Hemisphere swell near the east coast of North America.

The purpose of this paper is to document and describe the observations of long-period swell in the western North Atlantic Ocean and the meteorological conditions causing the swell.

The wave measurements are unusual for several reasons. First, they were made by many independently operating buoys with different hull types at different locations. This provides confidence in the measurements and shows how wave conditions vary with location. Second, the observations of such long-period swell are rare in the North Atlantic, and the reports may be used to improve modeling of the evolution of

Corresponding author address: Dr. Glenn D. Hamilton, NOAA, Chief, Data Systems, National Data Buoy Center, Stennis Space Center, MS 39529-6000.

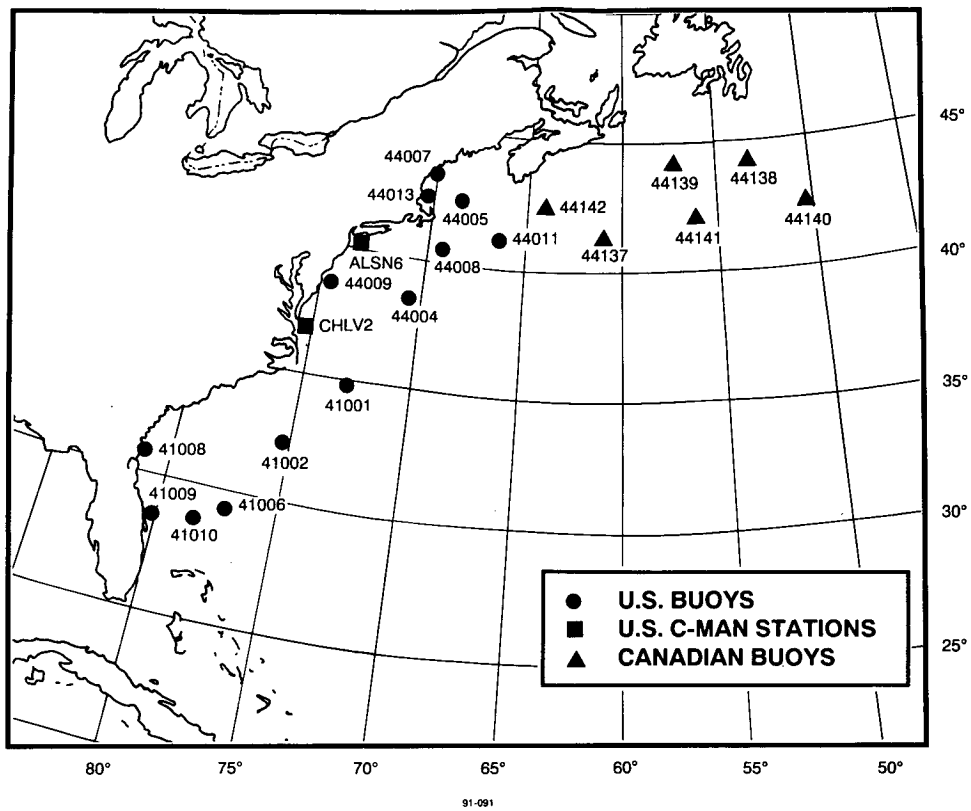

FIG. 1. Locations of buoys and C-MAN stations measuring long-period swell.

wind waves in the generating area into swell that propagates over long distances.

2. Wave measurements

Wave data were used from the stations listed in Table 1, which shows the station number, position, water depth, each buoy type, maximum 20-s-period energy measured (U.S. buoys), and highest significant wave height. Buoy locations are referenced by World Meteorological Organization station numbers.

NDBC wave measurements were made with onboard instrumentation consisting of a vertical accelerometer and electronics that produce estimates of nondirectional spectra. Details of the data collection and analysis procedures for NDBC wave systems have been described by Steele and Earle (1979). The basic wave sensor in these systems is a strapped-down accelerometer fixed in the buoy with its (single) measurement axis perpendicular to the buoy deck. Measured acceleration records are 20 min long with a sampling rate of 2.56 Hz. After appropriate signal conditioning, such as use of antialiasing filters, accelerometer records are digitized, and acceleration spectra are calculated by onboard microprocessors. Spectra are transmitted to shore hourly via GOES (Geostationary Operational Environmental Satellite). Acceleration spectra are corrected for low-frequency noise caused by strapping down the accelerometer, for filter responses during signal conditioning, and for buoy hull–mooring responses. Displacement spectra, which are standard wave spectra, are obtained from acceleration spectra by dividing the acceleration energy in each frequency band by the radian band center frequency to the fourth power. Wave spectra extend from 0.01 to 0.40 Hz in 0.01-Hz intervals, although spectra are not normally used for frequencies less than 0.03 Hz where there is negligible wind-generated wave energy. Twenty-four degrees of freedom are associated with each spectral estimate.

NDBC operational data buoys use strapped-down accelerometers because vertically stabilized accelerometers (e.g., gyroscope-type devices) are expensive and bulky. Hence, the heave acceleration sensed by the buoy, which tilts in response to the seaway, is not always aligned with the true vertical acceleration of the local wave surface. As a result, the acceleration spectra measured by NDBC buoys have small levels of excess low-frequency energy. Techniques have been developed and implemented to "correct" the spectra on shore prior

TABLE 1. Station information.

Station*	Latitude (°N)	Longitude (°W)	Water depth (m)	Type	Maximum 20-s-period energy (m^2 Hz^{-1})	Highest significant wave height (m)
			U.S. stations			
41001	34.9	73.0	4191	6-m NOMAD	0.75	1.0
41002	32.3	75.2	3660	6-m NOMAD	0.30	0.7
41006	29.3	77.4	1043	6-m NOMAD	0.50	0.6
41008	30.7	81.1	18	3-m discus	0.15	0.5
41009	28.5	80.2	41	3-m discus	0.10	0.4
41010	28.9	78.5	834	10-m discus	0.25	0.5
44004	38.5	70.6	3233	6-m NOMAD	2.40	1.1
44005	42.7	68.6	206	6-m NOMAD	0.85	0.9
44007	43.5	70.1	49	12-m discus	0.50	0.7
44008	40.5	69.4	61	12-m discus	1.20	1.1
44009	38.4	74.7	27	12-m discus	0.70	1.1
44011	41.1	66.6	93	6-m NOMAD	1.70	1.1
44013	42.4	70.8	33	12-m discus	0.50	0.5
ALSN6	40.5	73.8	18	C-MAN	0.80	0.9
CHLV2	36.9	75.7	12	C-MAN	0.87	1.1
			Canadian stations			
44137	41.2	61.2	4500	6-m NOMAD		1.2
44138	44.2	53.6	1500	6-m NOMAD		1.5
44139	44.3	57.4	1100	6-m NOMAD		1.5
44140	42.7	50.6	1500	6-m NOMAD		1.7
44141	42.1	56.1	4500	6-m NOMAD		1.4
44142	42.5	64.2	1500	6-m NOMAD		1.3

* These numbers are the World Meteorological Organization station location numbers. At different times, different individual buoys may be at these stations. Each C-MAN station is assigned an alphanumeric designator derived from its location.

to dissemination. These corrections decrease the amplitude of swell energy in the raw reported data. This is significant as it makes the detection of low-energy, long-period swell more difficult and emphasizes that the low-energy swell measured and reported on here is real and not an artifact. Previous computer simulations of accelerometer measurements (Earle and Bush 1982) addressed the use of strapped-down accelerometers.

C-MAN stations that measure waves use an infrared laser wave-height sensor (IR LWHS). This device employs a pulsed diode laser and photodiode detector along with the appropriate transmitter–receiver optics in a side-by-side configuration. The sensor is mounted in a fixed position above the water to provide perpendicular incidence of the laser beam on the water surface. Range is determined by measuring the propagation time of a 6-ns, 850-nm laser pulse to the water surface and back. A 1.5-kHz laser repetition rate permits averaging over a large number of pulses to improve range precision. The IR LWHS is discussed in Brown and Gustavson (1990).

The following information on the Canadian buoy wave-processing system was derived from Seastar (1991). The Canadian system has a sampling rate of 1 Hz with a burst duration of 34.13 min (2048 samples). There are eight blocks per burst (256 samples per block), and the blocks are not contiguous. The sensor signal is low-pass filtered with a single corner at 10 Hz to reduce aliasing due to noise, etc. A spectrum is calculated for each block. The spectra are ensemble averaged into a single, 128-band wave spectrum. The spectrum is corrected for the cosine taper effect. The spectrum between 2 and 30 s is corrected for the transfer function of the heave sensor. Band averaging is conducted on frequencies above the 0.1035–0.1074-Hz band, which gives a total of 42 frequency bands of wave data. Each band has a bandwidth of 0.003906 Hz. Dominant wave periods are then 32.0 s, 28.4 s, 25.6 s, 23.3 s, 21.3 s, 19.6 s, 18.2 s, etc.

3. Swell characteristics

Figure 2 shows the time history of spectral energy density in the low-frequency bands centered at 0.05 and 0.06 Hz at station 44004. Figure 3 gives the corresponding time history of significant wave height and dominant wave period. Significant wave height was computed from each spectrum by

$$H_s = 4(\text{total energy})^{1/2}, \quad (4)$$

where the total energy was obtained by integration of the spectrum over all frequencies, and equals the vari-

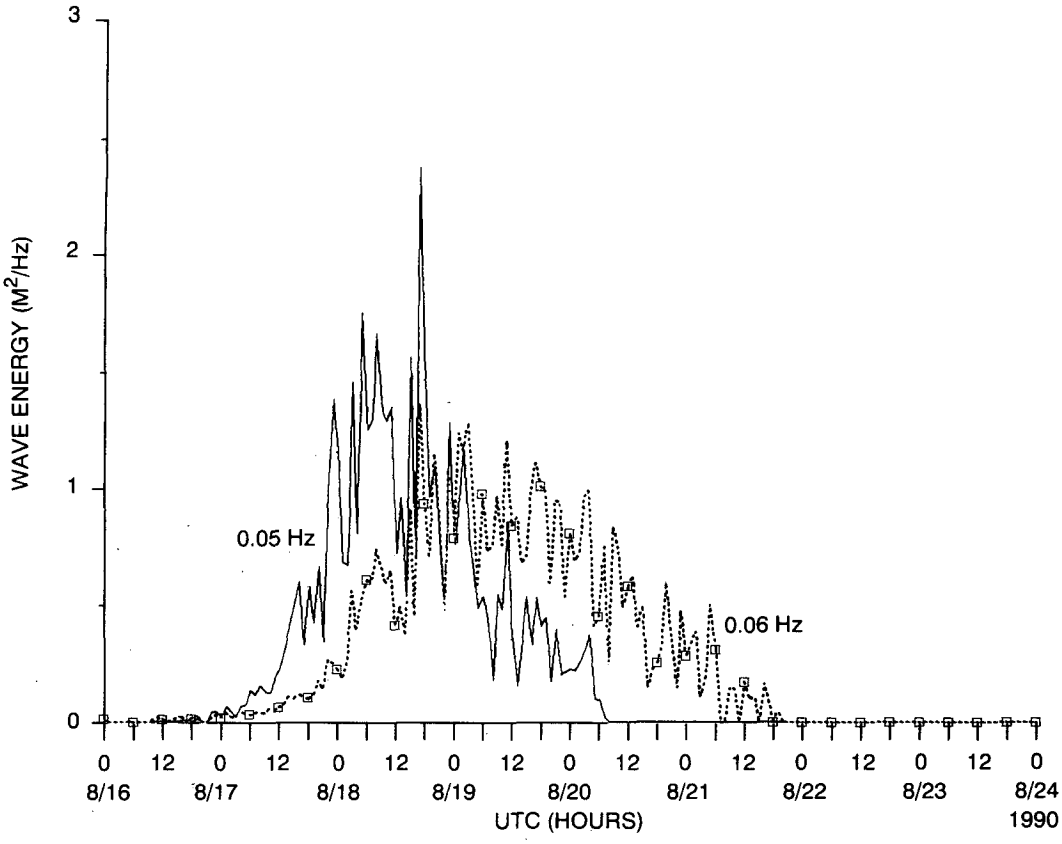

FIG. 2. Time-series history of low-frequency energy density at frequencies of 0.05 and 0.06 Hz at station 44004.

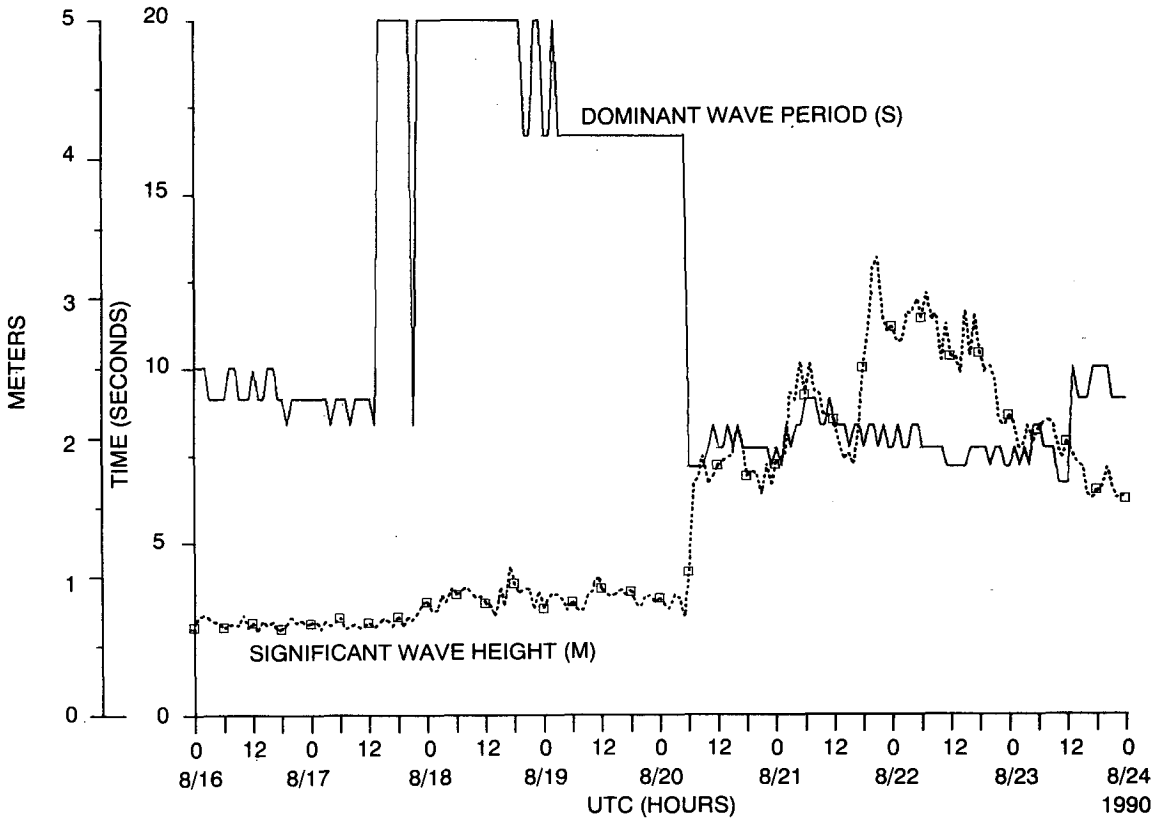

FIG. 3. Time-series history of dominant wave period and significant wave height at station 44004.

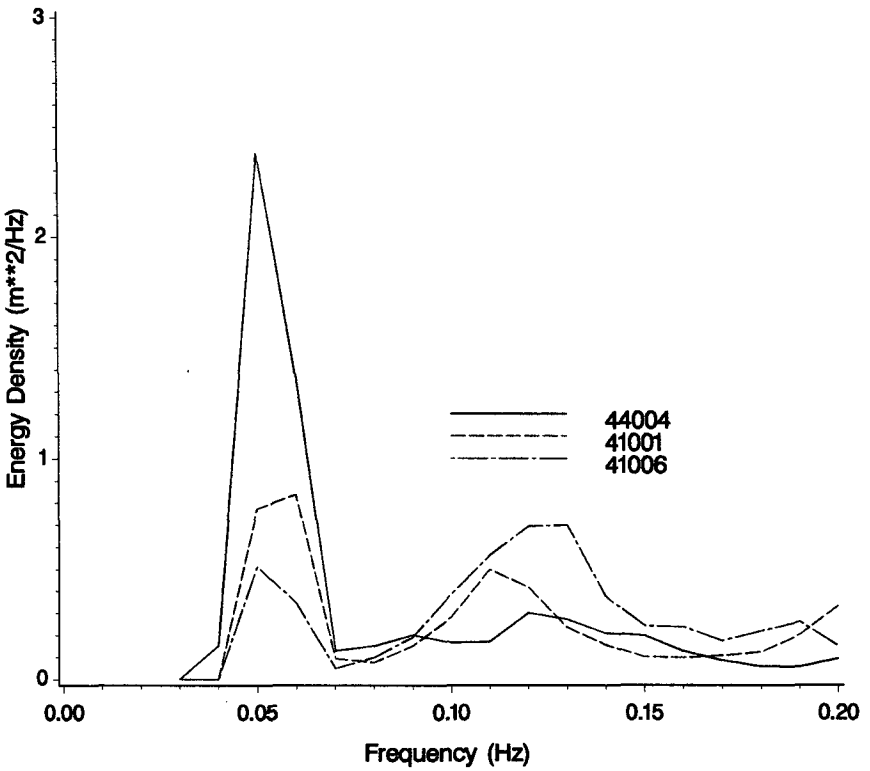

FIG. 4. Examples of wave spectra at time of maximum 0.05-Hz energy.

ance about the mean of the wave record. Because of finite spectral-width effects, spectrally calculated significant wave heights are typically a few percent higher than significant heights obtained by averaging the highest one-third waves in a time-series wave record (e.g., Longuet-Higgins 1980). Dominant wave period is defined as the period corresponding to the center frequency of the frequency band with maximum spectral energy density (i.e., 33.3 s, 25.0 s, 20.0 s, 16.7 s, etc.). The dominant wave-period plots are somewhat "jumpy" because of the 0.01-Hz resolution of the frequency bands. Figure 4 shows examples of wave spectra at the times of highest 0.05-Hz wave energy at stations 44004, 41001, and 41006. The decrease in energy from north to south along the chain is evident.

Wave energy travels along great-circle routes with a frequency-dependent group velocity c_g of

$$c_g(f) = \frac{g}{4\pi f}, \tag{5}$$

where g is the acceleration due to gravity (e.g., Neumann and Pierson 1966). Swell generated at time t_0 arrives at a location a distance d away at the time t_a given by

$$t_a = t_0 + \frac{d}{c_g}. \tag{6}$$

Differentiation of Eq. (6) shows that the distance can be calculated from

$$\frac{dt_a}{df} = \frac{4\pi d}{g} \approx \frac{t_2 - t_1}{f_2 - f_1}, \tag{7}$$

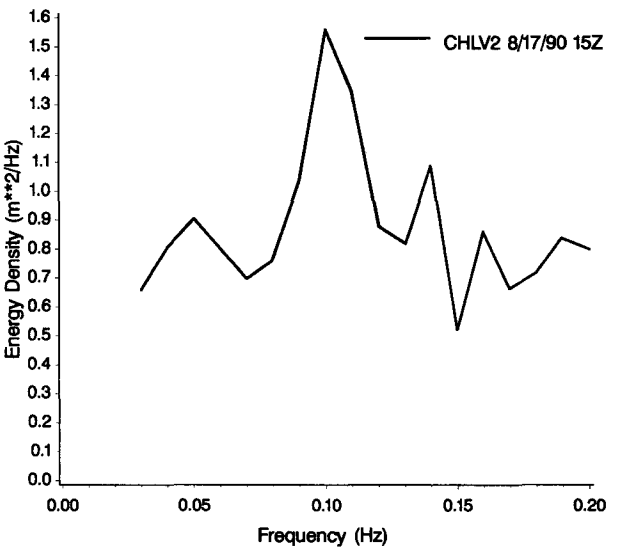

FIG. 5. Wave spectra at time of maximum 0.05-Hz energy at station CHLV2.

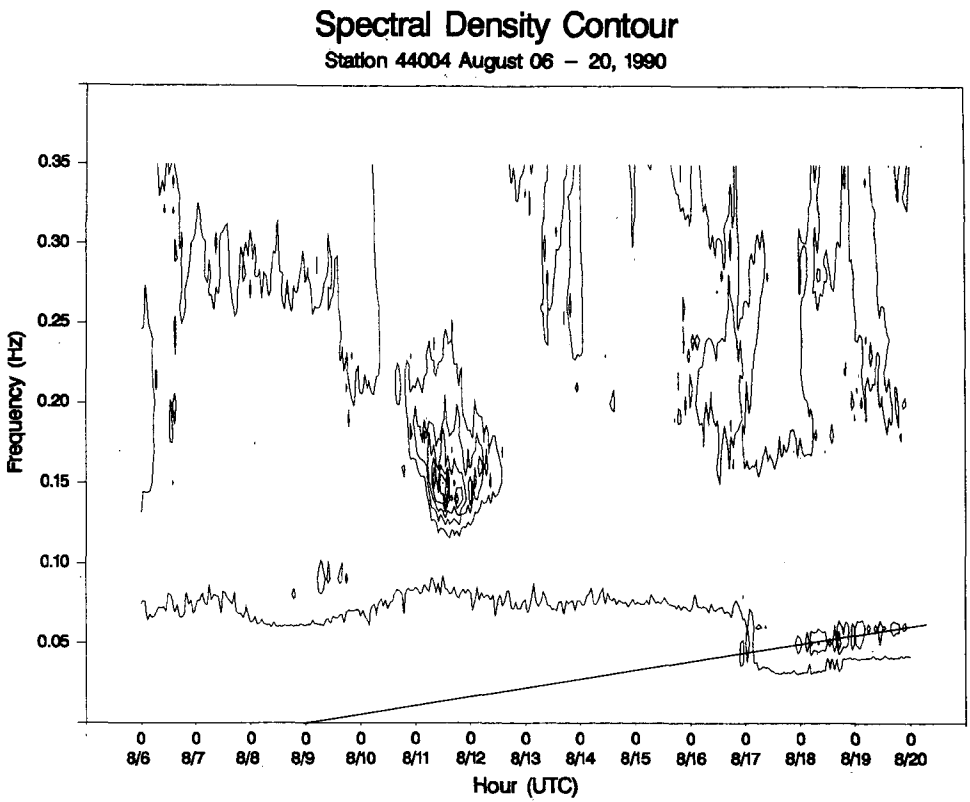

FIG. 6. Contour plot of energy density as a function of frequency and time for station 44004.

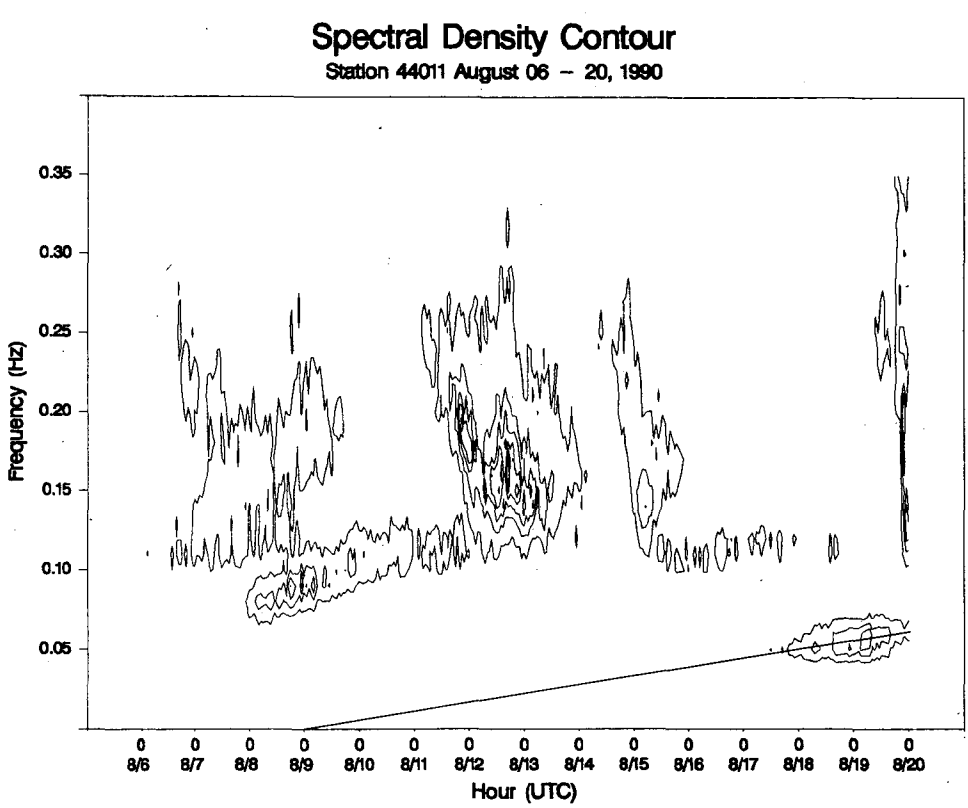

FIG. 7. Contour plot of energy density as a function of frequency and time for station 44011.

where t_1 and t_2 are arrival times of energy at frequencies f_1 and f_2, respectively. Because of the dispersive nature of swell propagation, the difference in arrival times of energy at different frequencies can be used to calculate propagation distances. Similarly, if the distance and arrival time are known, Eq. (6) can be used to obtain the generation time.

The highest significant wave height while the long-period swell was present of 1.7 m was recorded at Canadian station 44140 at the northeastern tip of the chain of stations (Table 1 and Fig. 1). The significant wave heights generally decreased southwestward in the entire network. For the buoy stations reporting wave spectral data (U.S. stations), the buoy at deep-water station 44004 reported the highest level of 20-s-period energy (Table 1), and the energy decreased to the southwest along the network. This strongly suggests that the main path of the swell track was closer to the Canadian buoys than the U.S. network. Because of their unique information, stations 44140 and 44004 are used in several calculations.

The propagation distance can normally be determined by using the difference in arrival times of the two frequencies in Eq. (7). In Fig. 2, however, the onset of energy at 0.05 and 0.06 Hz is unclear at 44004, although the cessation of the energy at these frequencies

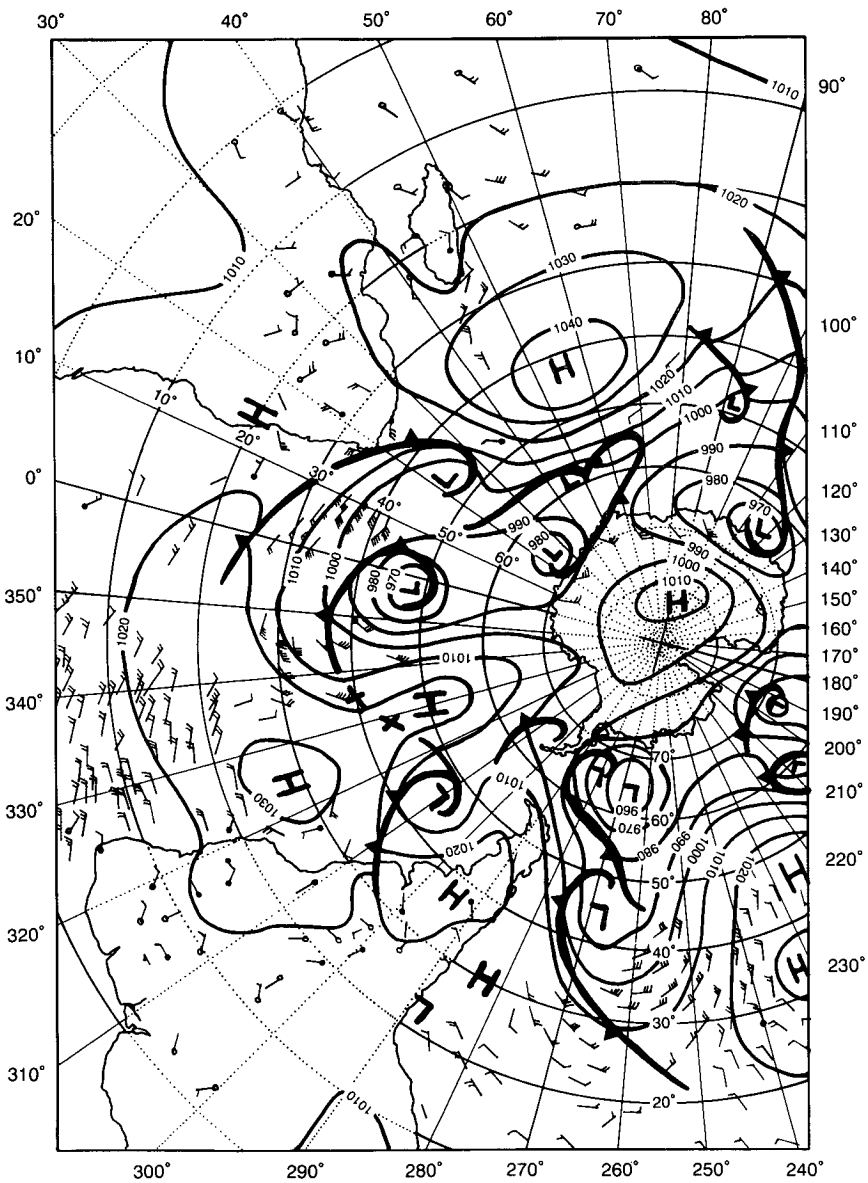

FIG. 8. South Polar surface synoptic weather chart for 1200 UTC 8 August 1990.

is more precise. The time difference between the cutoff of the 0.05-Hz energy and the end of the 0.06-Hz energy is 36 h, and if this is applied to Eq. (7), the propagation distance is about 10 000 km.

Another approach for estimating propagation distance may be through the difference in arrival times of swell with different dominant wave periods. A dominant wave period of 20 s (0.05 Hz) first occurred at 44004 at 1400 UTC 17 August (t_1) and was present until 0200 UTC 19 August (t_2) (Fig. 3) when the dominant period changed to 16.7 s (0.06 Hz). The time difference was again 36 h, giving a propagation distance of about 10 000 km.

The Canadian buoys reported wave spectra, but unfortunately the data were not archived. The hourly weather observations, reported in FM 13 SHIP code over the World Meteorological Organization Global Telecommunications System, were available, however, and included reports of significant wave height and dominant wave period (to the nearest second). All of the Canadian buoys reported dominant periods of 20 s (0.050778 Hz) lasting from 12 to 16 h until the next lower dominant wave period of 18 s (0.054684 Hz) arrived. Using an average of 14 h for ($t_2 - t_1$) and 0.003906 Hz for ($f_2 - f_1$), the propagation distance is estimated to be 10 000 km.

An interesting event was the measurement of energy greater than 30 s. The buoys at stations 44138 and 44139 began reporting a 32-s dominant period as early as 10–11 August. These stations have two of the shallowest moorings (1100 m). All of the other Canadian buoys measured 32-s dominant periods before reporting 20-s dominant periods, except station 44137, which is in deep water (4500 m) and at the southwest end of the array.

There were no reports of dominant wave period greater than 20 s on the U.S. buoys. Some buoy stations, such as 44004 in Fig. 4, measured 25-s energy. None of the deep-water buoys measured 33.3-s-period energy, although 33.3-s wave energy occurred at the shallow-water sites. This was most evident at CHLV2, the C-MAN station at Chesapeake Light, Virginia, which has an infrared laser wave-height sensor (Fig. 5). This plot was at the time of arrival of the maximum value of 33.3-s-period energy.

The measurement of the 20-s dominant period occurred first at 44140, which is the easternmost station of the whole array, and then showed up at stations progressively to the west. Using the group velocity (56 km h^{-1}) and multiplying it by the number of hours of time difference between the first measurement of dominant period of 20 s at 44140 and its first occurrence at subsequent stations, an arc can be drawn from each station that would approximate a loci of locations along which the energy from the wave-front train would lie at the time it impacted 44140. Visually, it is apparent that the wave train was advancing toward the buoys from the southeast. Interpolating and drawing a line along the arcs, the swell train seems to be coming from about 140°–145° (southeast).

The peak 20-s energy occurred at 1700 UTC 18 August at both 44004 (Fig. 2) and 44011. When a line

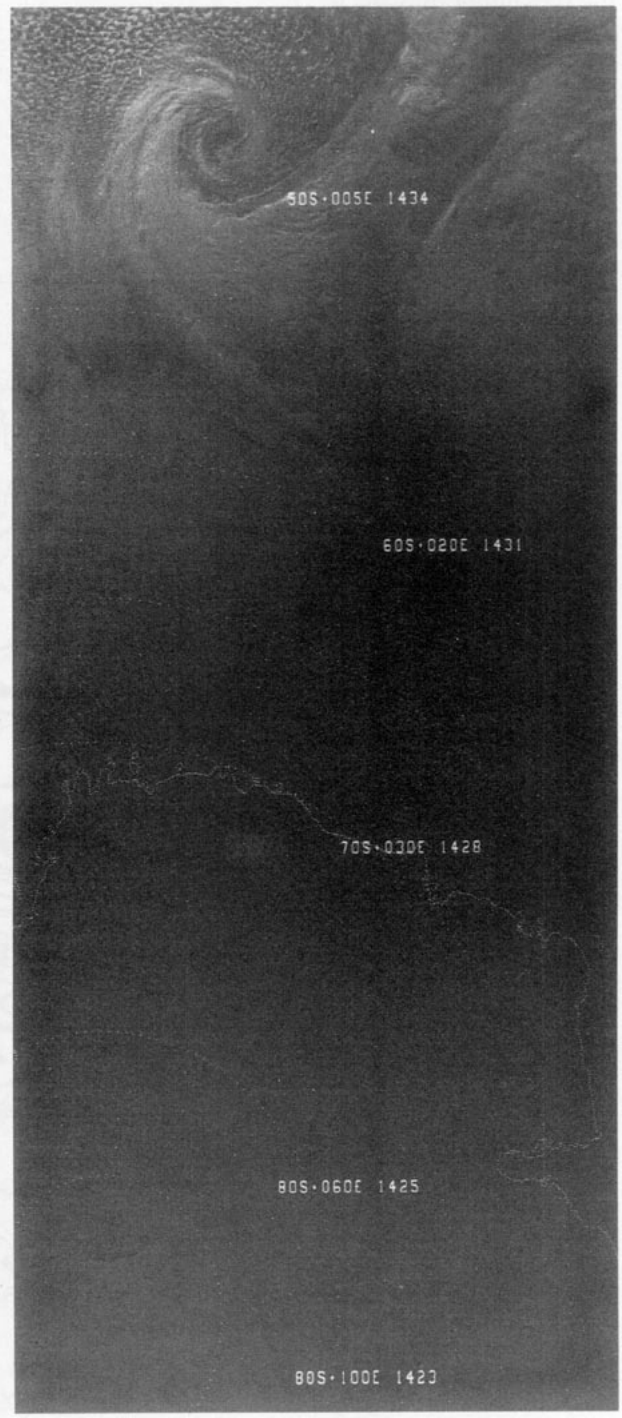

FIG. 9. NOAA polar-orbiting satellite visible image 1420 UTC 8 August 1990.

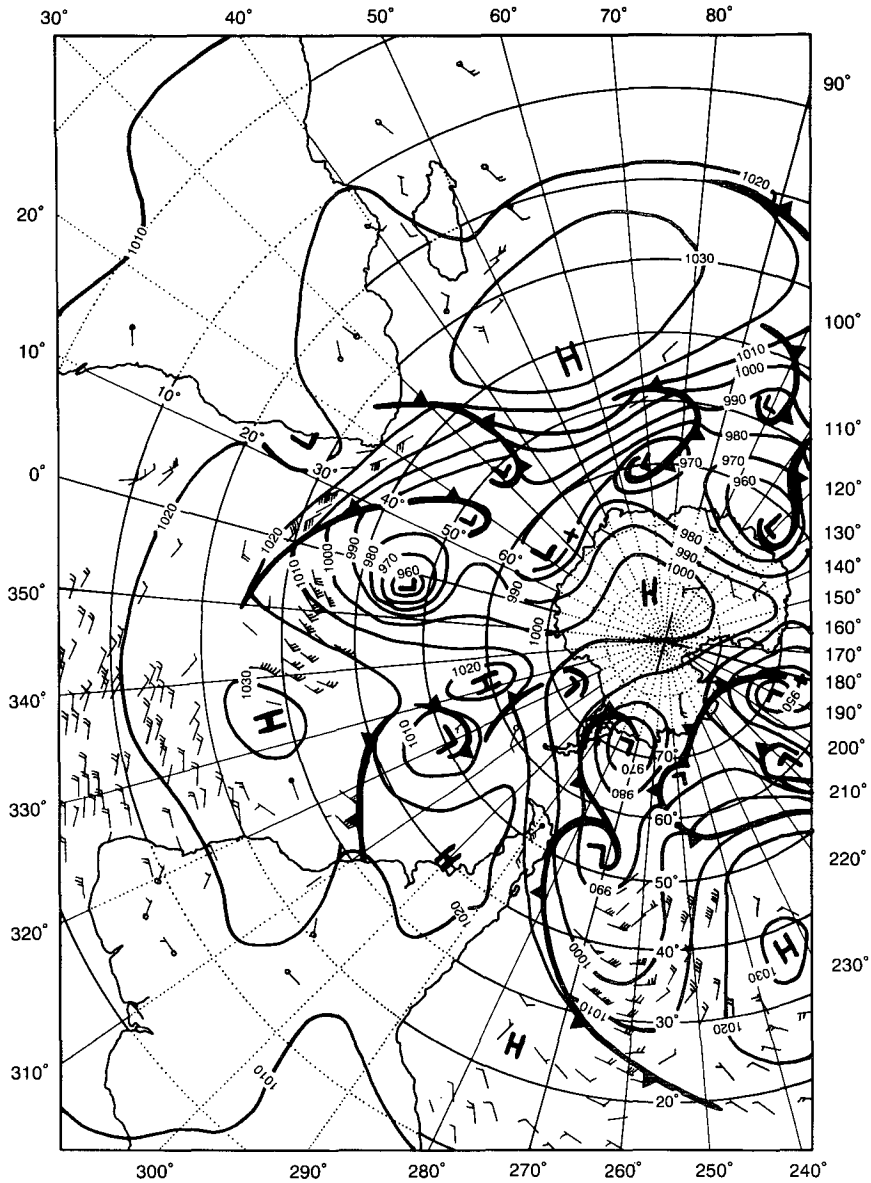

FIG. 10. As in Fig. 8 but for 0000 UTC 9 August 1990.

representing the wave front is drawn between the two stations, the orthogonal to the wave front, which would represent the swell track, is approximately 140°. With two techniques estimating the swell train to be coming from nearly the same direction, it would seem reasonable to assume that it was arriving from the southeast. When applying this direction to a great-circle path on a globe, the swell appears to be coming through the gap between the eastern tip of South America and the western edge of Africa.

The generation time of the swell can be obtained from Eq. (6). The arrival time of the first 20-s-period energy at station 44004 was on 16 August (Fig. 2). Using 10 000 km for d, 56 km h^{-1} for c_g, and 16 August for t_a, then t_0 is estimated as being 9 August. As no wave-spectral data were available for the Canadian buoys, this calculation cannot be made for 44140.

Figures 6 and 7 are automated contour plots of energy density as a function of frequency and time for 44004 and 44011 (similar plots in past literature have been hand drawn). The contours are at intervals of 0.8 m^2 Hz^{-1}. On the time axis, the ticks designate 0000 UTC. Energy peaks associated with a given event appear as slanting ridges. Dispersion theory predicts (Munk et al. 1963) that these ridges should be straight. The intersection of the ridge line at the axis of $f = 0$

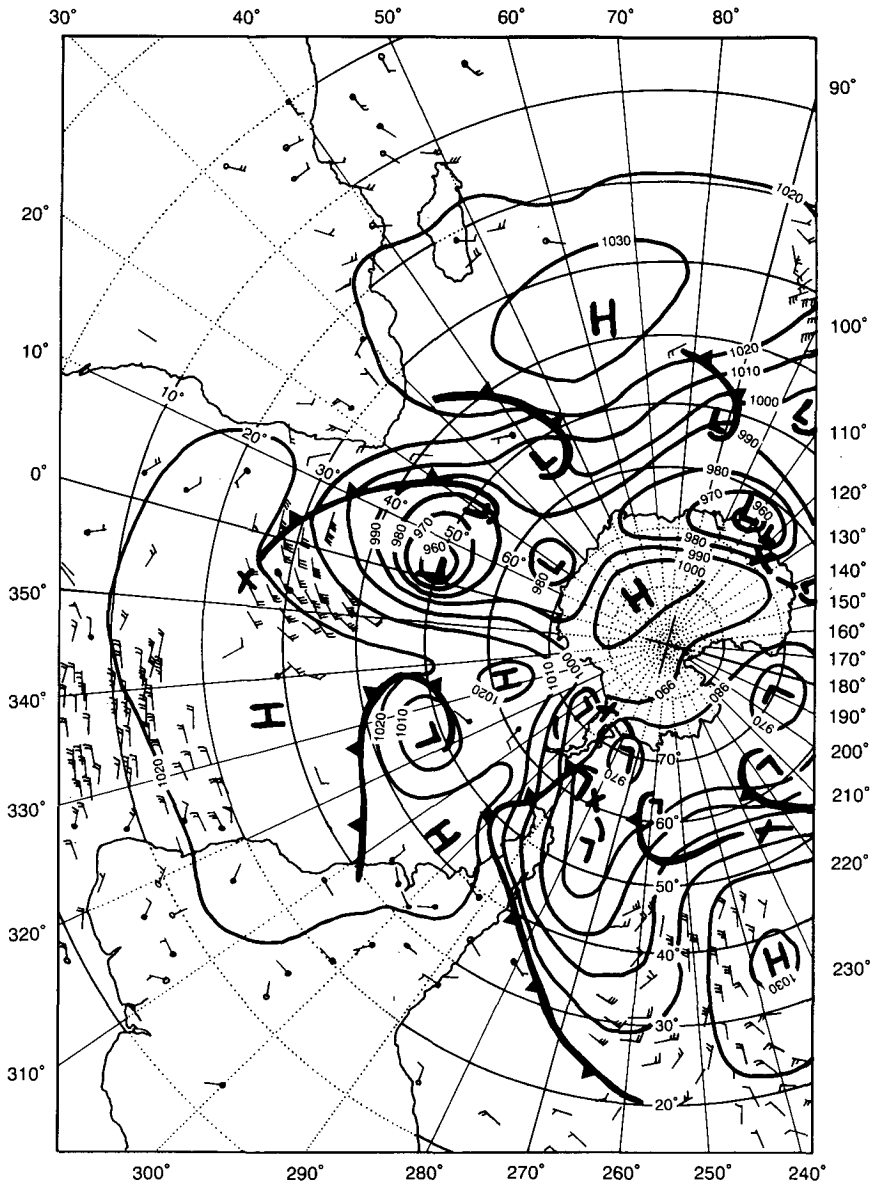

FIG. 11. As in Fig. 8 but for 1200 UTC 9 August 1990.

gives the time origin at the source of the swell event (Cartwright et al. 1977). Figure 6 shows long-period energy first appearing at 44004 at 2200 UTC 16 August with an energy packet sloping slightly up to the right on subsequent days. When a line is drawn along the ridge line of the axis of the packet, the intersection of the line with the $f = 0$ axis is about 9 August. When the technique is applied to Fig. 7, for 44011, the intersection is also near 9 August.

4. Meteorological situation

Assuming that the center of the swell train impacted near buoy station 44140, that it was arriving from 140° to 145° on a great-circle path, and that the distance to the origin of the swell was about 10 000 km, then the location of the generating area was probably in the general vicinity of 50°S, 5°E.

To investigate the meteorological conditions, polar-stereographic weather charts centered on the South Pole were obtained from the Australian Bureau of Meteorology. Figure 8, the analysis for 1200 UTC 8 August 1990, shows a deep low with a central pressure less than 970 hPa centered near 48°S, 2°W (longitude 358° on the chart). Satellite-derived winds as far as 1000 km to the west are indicated to be 40 kt (21 m s^{-1}). It would seem reasonable to assume the the winds near

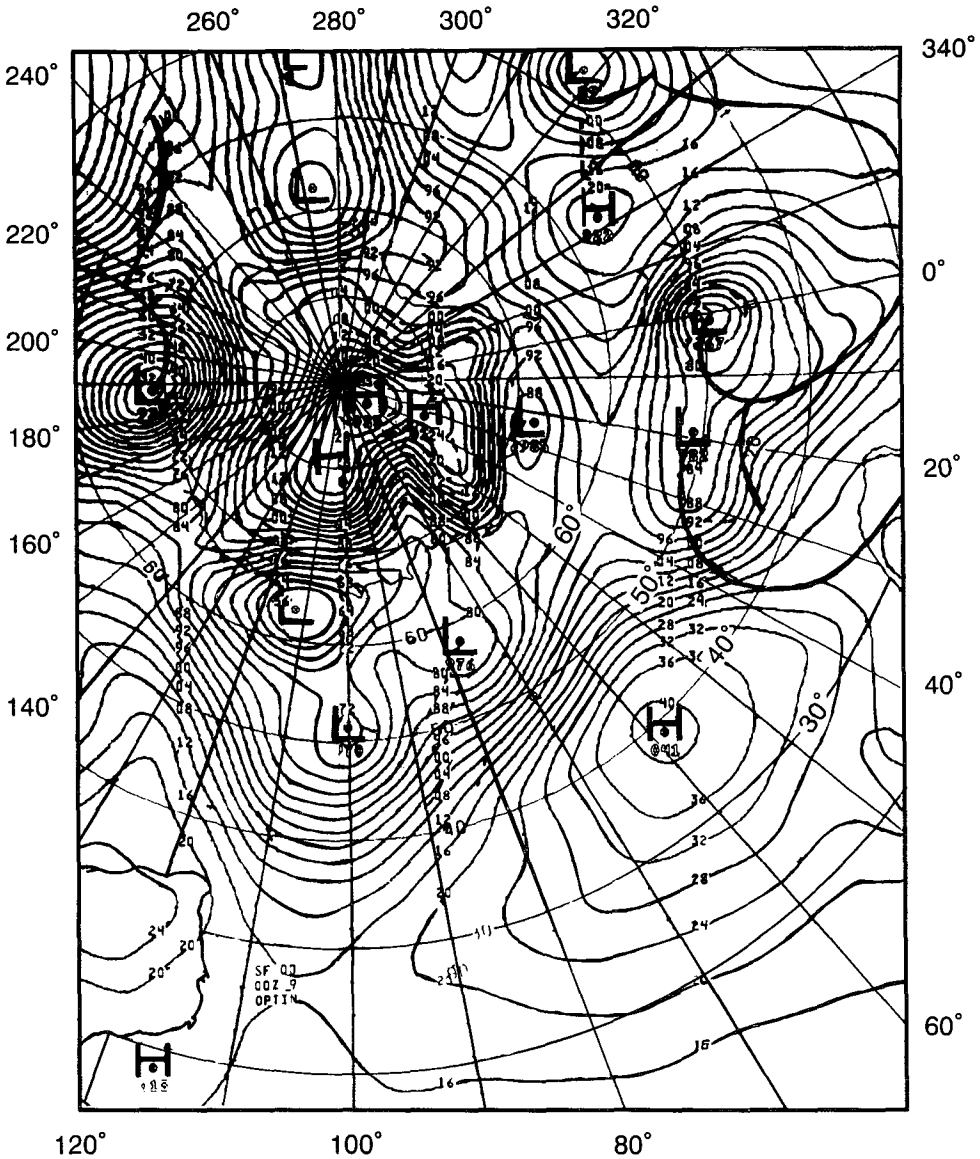

FIG. 12. U.S. National Weather Service surface weather analysis for 1200 UTC 8 August 1990.

the center, where the pressure gradient is tighter, would be near 50 kt (26 m s^{-1}). The fetch extends from the edge of the Antarctic continent northward to about 45°S, although the southernmost extent is governed by the ice edge. The Navy–NOAA Joint Ice Center (JIC) analyses on 6 and 13 August showed the northern ice limit to be near 58°S, so the effective fetch was well over 1000 km. In Fig. 9, a visible satellite image at 1420 UTC 8 August; the storm is evident. Figure 10, the analysis for 0000 UTC 9 August, shows that the storm had been nearly stationary and had intensified further to below 960 hPa with an extremely tight pressure gradient to the west. No wind reports were provided with this analysis, but storms of this strength have been found to have winds of greater than 30 m s^{-1} (e.g., Earle et al. 1984). The analysis for 1200 UTC 9 August, given in Fig. 11, shows the slow-moving storm with the same tight pressure gradient. Figure 12, an analysis at 1200 UTC 9 August by the U.S. National Weather Service (NWS), gives a slightly different view of the low center, but shows the low to be in about the same position as the Australian analysis. Surface pressure analyses may have severe deficiencies in data-sparse Southern Ocean areas (Dexter 1980). Even as suspect as the analyses are, it appears that the storm existed for about 3 days in the same general vicinity.

Mognard et al. (1982) analyzed selected Seasat radar altimeter passes over the Southern Ocean and found

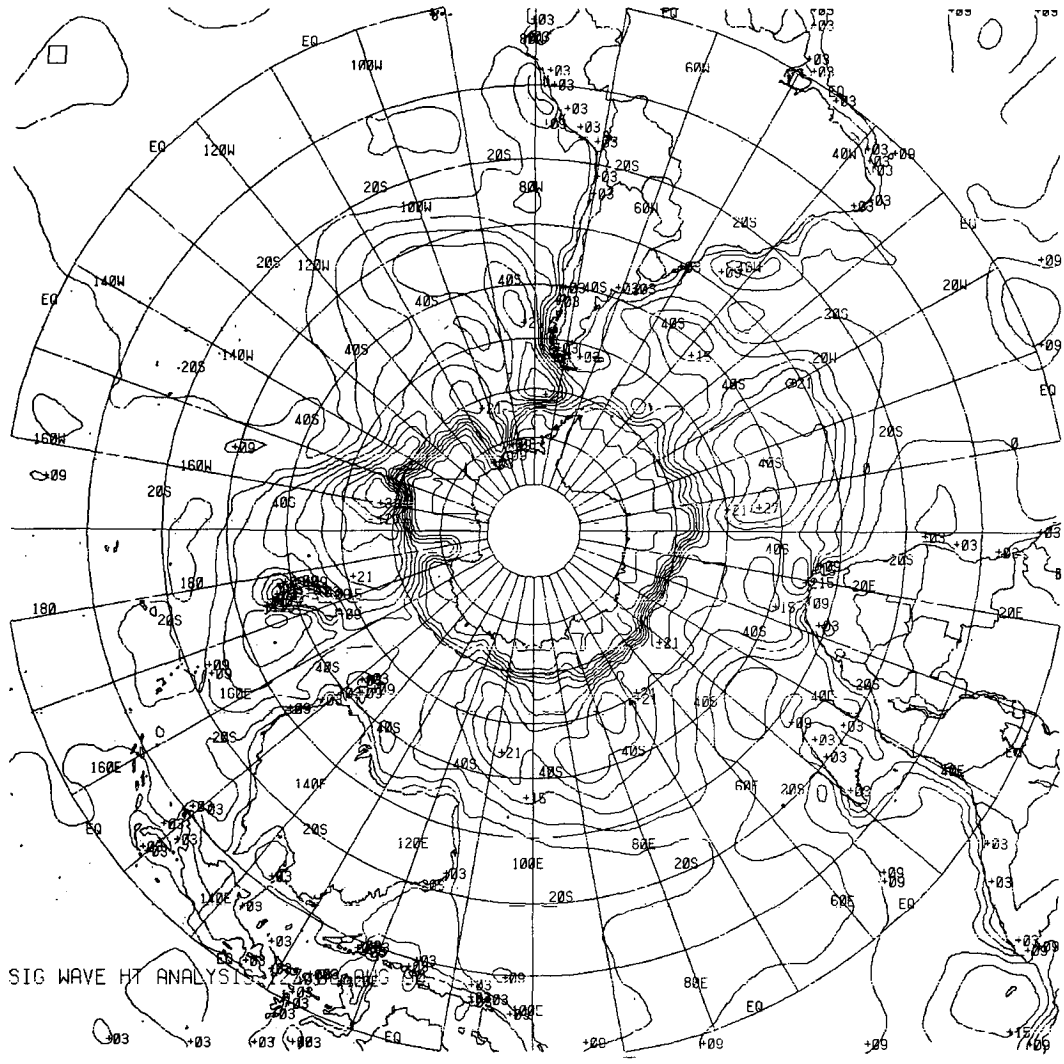

FIG. 13. Significant-wave-height analysis for 1200 UTC 8 August

that most of the oceans had significant wave heights of approximately 2–4 m during the Antarctic winter, making them the roughest of the world's oceans. Also, in all parts of the Southern Ocean, families of very large wind waves (10–12 m) and swell (8–10 m) are frequently generated by strong atmospheric storm systems.

Figure 13 shows the U.S. Navy Fleet Numerical Oceanography Center (FNOC) Southern Hemisphere significant-wave-height analysis for 1200 UTC 8 August 1990 (the JIC-defined ice edge around the continent is also shown). The analysis is part of the output of the Global Spectral Ocean Wave Model (GSOWM) (Clancy et al. 1986) that is routinely run at FNOC. In the general vicinity of the storm, shown in Fig. 8, significant wave heights of 21 ft (6 m) to 27 ft (8 m) are analyzed. The GSOWM-determined dominant wave periods for the Northern Hemisphere locations of the buoys for 17–20 August 1990 did not show any 20-s-period energy present. Personnel at FNOC extracted wave-spectra plots near the buoys for the same time interval and there was no 20-s-period energy calculated by the model (Clancy, personnel communication). For some reason, the GSOWM did not propagate the swell from the Southern Hemisphere, and the cause is being investigated. Figure 14 is an azimuthal equidistant projection showing the great-circle path of the swell from the storm source to the area of the Canadian buoys.

5. Summary

In August 1990, all 21 wave-measuring stations of the United States and Canadian data buoy networks

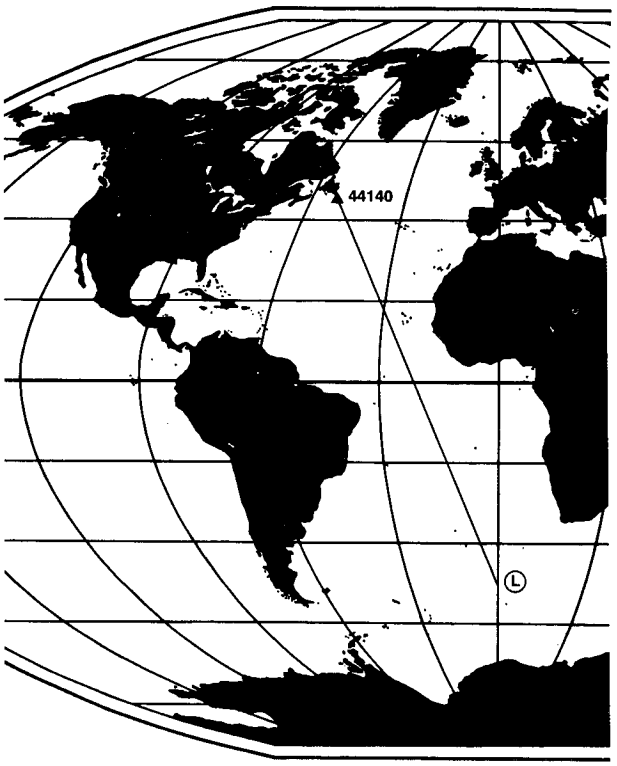

FIG. 14. Azimuthal equidistant projection with the 142.5°T great-circle route between the easternmost Canadian buoy station 44140 and the principal storm source indicated.

reported long-period, low-amplitude swell. The energy was first evident at the Canadian buoys at the northeast tip of the chain and then appeared progressively down the network to the southwest. The situation of low significant wave heights along the entire eastern seaboard and the recording of dominant wave periods of long-period swell at many of the stations was very unusual. This study is believed to be the first documentation of such an event. Long-period swell in the western North Atlantic has probably occurred in the past but was most likely masked by higher frequency wind-wave energy.

Using various techniques, the source of the long-period swell arriving in the western North Atlantic was estimated to be near the Antarctic continent, a distance of some 10 000 km. The actual storm that generated the swell was found to be located in the same general vicinity as expected. The storm was a deep, intense, slow-moving system that had a very tight pressure gradient, oriented in a south-to-north direction, on the west side of the storm. The fetch was over 1000 km in length to the north of the ice edge. Propagation of the swell was consistent with classical concepts of energy propagation at group velocities along great-circle routes. The swell took about 7 days to reach the buoy network.

It is considered significant that the swell was measured by independently operating stations with different hull types, sensors (accelerometers on buoys and laser wave-height instruments on C-MAN stations), and different electronic payloads and wave-spectra calculation schemes on the U.S. and Canadian stations. This provides confidence in the wave measurements and a description of how wave conditions vary with location.

The determination of the direction to the storm source is a rather involved process. If the stations were equipped with directional wave sensors, it would facilitate resolving the path of the swell. Directional wave data may have helped, too, in determining if there were any refraction of the swell trains as they crossed the Gulf Stream. NDBC operates a number of directional wave buoys, primarily for users who reimburse NDBC for deploying the buoys, but there were no deep-water directional wave buoys in the Atlantic at the time of this event. Wang and Carolan (1991) discuss the use of NDBC directional wave data in the Pacific. The event described in this paper illustrates the probable usefulness of directional wave measurements.

Finally, the database from the data buoys during the period of this study represents an important resource that can be used for projects involving wave-generation theories and development of improved global numerical wave models. There is presently little information to verify how well such models forecast or hindcast waves generated by Southern Ocean storms.

Acknowledgments. The author would like to thank the personnel of the National Data Buoy Center and the support contractor, Computer Sciences Corporation, for their assistance in the preparation of many data analysis products. In particular, Mr. David Gilhousen provided many essential graphics displays. Several individuals, including Dr. Willard J. Pierson, Jr., Dr. Marshall D. Earle, Dr. W. Wang, and Mr. Kenneth E. Steele, provided many helpful suggestions and comments.

REFERENCES

Barber, N. F., and F. Ursell, 1948: The generation and propagation of ocean waves and swell. *Phil. Trans. Roy. Soc. London,* **A240,** 527–560.

Brown, H., and R. Gustavson, 1990: Infrared wave height sensor. *Proc. Mar. Instr. '90,* San Diego, Mar. Technol. Soc., 141–150.

Cartwright, D. E., J. S. Driver, and J. E. Tranter, 1977: Swell waves at Saint Helena related to distant shores. *Quart. J. Roy. Met. Soc.,* **103,** 655–683.

Clancy, R. M., J. E. Kaitala, and L. F. Zambresky, 1986: The Fleet Numerical Oceanography Center Global Spectral Ocean Wave Model. *Bull. Amer. Meteor. Soc.,* **67,** 498–512.

Dexter, P. E., 1980: The forecasting of long-period swell. *Trans. Instit. of Eng., Australia,* **CE 22,** No. 2, 132–140.

Earle, M. D., and K. A. Bush, 1982: Strapped-down accelerometer effects on NDBO wave measurements. *Proc. Oceans* '82, Washington D.C., Mar. Technol. Soc. and IEEE, 838–848.

——, ——, and G. D. Hamilton, 1984: High-height long-period ocean waves generated by a severe storm in the northeast Pacific Ocean during February 1983. *J. Phys. Oceanogr.,* **14,** 1286–1299.

Ewing, J. A., 1971: The generation and propagation of sea waves. *Dynamic Waves in Civil Engineering.* Wiley Interscience, 43–56.

Hamilton, G. D., 1986: National Data Buoy Center programs. *Bull. Amer. Meteor. Soc.,* **67,** 411–415.

Longuet-Higgins, M. S., 1980: On the distribution of the heights of sea waves: Some effects of nonlinearity and finite band width. *J. Geophys. Res.,* **85,** 1519–1523.

Mitsuyasu, H., 1981: Directional spectra of ocean waves in generation area. *Proc. Directional Wave Spectra Applications.* Berkeley, California, Amer. Soc. Civ. Eng., 87–101.

Mognard, N. M., W. J. Campbell, R. E. Cheney, J. G. Marsh, and D. B. Ross, 1982: Southern ocean waves and winds derived from Seasat altimeter measurements. *Wave Dynamics and Radio Probing of the Ocean Surface,* Plenum, 1736–1744.

Munk, W. H., G. R. Miller, F. E. Snodgrass, and N. F. Barber, 1963: Directional recording of swell from distant storms. *Phil. Trans. Roy. Soc. London,* **A255,** 505–584.

Neumann, G., and W. J. Pierson, 1966: *Principles of Physical Oceanography.* Prentice-Hall, 276.

Pierson, W. J., G. Neumann, and R. W. James, 1955: Practical methods for observing and forecasting ocean waves by means of wave spectra and statistics. H. O. Publ. 603, U.S. Navy Hydrographic Office, Washington, D.C.

Seastar, 1991: Seastar Instruments Operations/Maintenance/Reference Manual for 1991 NOMAD ZENO Payloads, Seastar Instruments Ltd., Sidney, B.C. Canada.

Snodgrass, F. E., G. W. Groves, K. F. Hasslemann, G. R. Miller, W. H. Munk, and W. H. Powers, 1966: Propagation of ocean swell across the Pacific. *Phil. Trans.* **A259,** 431–497.

Steele, K. E., and M. D. Earle, 1979: The status of data produced by NDBO Wave Data Analyzer (WDA) systems. *Proc. Oceans '79,* San Diego, Mar. Technol. Soc. and IEEE, 212–220.

Wang, D. W., and R. Carolan, 1991: Estimation of swell direction by a small discus buoy in high seas. Preprints, *Fifth Conf. on Meteorology and Oceanography of the Coastal Zone,* Miami, Amer. Meteor. Soc., 53–59.